ELECTRONIC SUPPORTING INFORMATION (ESI)

Heterometallic clusters based on an uncommon asymmetric "V-shaped" $[Fe^{3+}(\mu\text{-}OR)Ln^{3+}(\mu\text{-}OR)_2Fe^{3+}]^{6+}$ (Ln = Gd, Tb, Dy, Ho) structural core and the investigation of the slow relaxation of the magnetization behaviour of the $[Fe_2Dy]$ analogue

Maria Savva,[a] Dimitris I. Alexandropoulos,[a] Michael Pissas,[b] Spyros P. Perlepes,[c] Constantina Papatriantafyllopoulou,*[a†] Yiannis Sanakis,*[b] Anastasios J. Tasiopoulos*[a]

[a]*Department of Chemistry, University of Cyprus, 1678 Nicosia, Cyprus.*
E-mail: atasio@ucy.ac.cy
[b]*Institute of Nanoscience and Nanotechnology, NCSR "Demokritos", 15341 Aghia Paraskevi, Athens, Greece. E-mail: i.sanakis@inn.demokritos.gr*
[c]*Department of Chemistry, University of Patras, 26504 Patras, Greece.*
†Current address: School of Biological and Chemical Sciences, College of Science and Engineering, University of Galway, University Road, H91 TK33 Galway, Ireland. E-mail: constantina.papatriantafyllopo@universityofgalway.ie

Table of Contents

Single crystal X-Ray crystallography

Table S1. Crystal data and structural refinement parameters for compounds **1**·MeCN/Gd, **1**·MeCN/Tb, **1**·MeCN/Dy and **1**·MeCN/Ho

Identification code	**1**·MeCN/Gd	**1**·MeCN/Tb	**1**·MeCN/Dy	**1**·MeCN/Ho
Empirical formula	$C_{58}H_{48}ClGdFe_2N_8O_{15}$	$C_{58}H_{48}ClTbFe_2N_8O_{15}$	$C_{56}H_{45}ClDyFe_2N_7O_{15}$	$C_{58}H_{48}ClHoFe_2N_8O_{15}$
Formula weight	1401.44	1403.11	1365.64	1409.12
Temperature / K	104.3(6)	105(4)	105(2)	104(1)
Wavelength / Å	1.54184	1.54184	1.54184	1.54184
Crystal system	Monoclinic	Monoclinic	Monoclinic	Monoclinic
Space group	C 2/c	C 2/c	C 2/c	C 2/c
a/Å	36.202 (2)	36.2532(8)	36.1248(7)	36.162 (2)
b/Å	13.6502(5)	13.6224(3)	13.6090(3)	13.6340(5)
c/Å	23.4533(7)	23.4474(4)	23.3954(4)	23.3820(6)
β/°	94.603(3)	94.717(2)	94.628(2)	94.710(3)
Volume / $Å^3$	11552.6(7)	11540.4(4)	11464.2(4)	11489.2(6)
Z	8	8	8	8
Density (calculated) / Mg/m^3	1.612	1.615	1.582	1.629
Absorption coefficient / mm^{-1}	12.356	10.962	11.917	7.529
F(000)	5640	5648	5480	5664
Crystal size / mm^3	0.13 x 0.04 x 0.02	0.28 x 0.03 x 0.02	0.08 x 0.016 x 0.011	0.09 x 0.013 x 0.010
Theta range for data collection / °	3.462 to 66.991	3.783 to 66.999	3.472 to 66.993	3.466 to 66.997
Index ranges	-28 ≤ h ≤ 43 -14 ≤ k ≤ 16 -28 ≤ l ≤ 27	-43 ≤ h ≤ 43 -16 ≤ k ≤ 16 -22 ≤ l ≤ 27	-37 ≤ h ≤ 43 -16 ≤ k ≤ 16 -27 ≤ l ≤ 27	-42 ≤ h ≤ 43 -16 ≤ k ≤ 15 -27 ≤ l ≤ 19
Reflections collected	21252	21089	22211	20925
Independent reflections / R(int)	10272 / [R(int) = 0.0428]	10250 / [R(int) = 0.0317]	10183 / [R(int) = 0.0322]	10213 / [R(int) = 0.0377]

Reflections with $I>2\sigma(I)$	8520	8952	8668	8151
Completeness to theta = 66.99° / %	99.8	99.7	99.8	99.8
Absorption correction	Semi-empirical from equivalents	Semi-empirical from equivalents	Semi-empirical from equivalents	Semi-empirical from equivalents
Refinement method	Full-matrix least-squares on F^2	Full-matrix least-squares on F^2	Full-matrix least-squares on F^2	Full-matrix least-squares on F^2
Data / restraints / parameters	10272 / 0 / 767	10250 / 0 / 767	10183 / 0 / 739	10213 / 0 / 767
Goodness-of-fit on F^2	0.979	1.054	1.004	1.028
Final R indices [I>2sigma(I)]	R_1[a] = 0.0463	R_1 = 0.0390	R_1 = 0.0366	R_1 = 0.0468
	wR_2[b] = 0.1221	wR_2 = 0.1097	wR_2 = 0.0983	wR_2 = 0.1251
R indices (all data)	R_1 = 0.0574	R_1 = 0.0452	R_1 = 0.0456	R_1 = 0.0621
	wR_2 = 0.1293	wR_2 = 0.1146	wR_2 = 0.1033	wR_2 = 0.1338
Largest diff. peak and hole / e Å^{-3}	1.208 and -0.701	0.831 and -1.125	0.797 and -0.688	0.832 and -1.094

[a] $R_1 = \Sigma(||F_o| - |F_c||)/\Sigma|F_o|$. [b] $wR_2 = [\Sigma[w(F_o^2 - F_c^2)^2]/\Sigma[w(F_o^2)^2]]^{1/2}$, $w = 1/[\sigma^2(F_o^2) + [(ap)^2 + bp]$, where $p = [\max(F_o^2, 0) + 2F_c^2]/3$.

Table S2. Shape measures of the 9-coordinate Gd1 – Ho1 coordination polyhedra in **1**·MeCN/Gd, **1**·MeCN/Tb, **1**·MeCN/Dy and **1**·MeCN/Ho, respectively

Polyhedron[a]	Gd1	Tb1	Dy1	Ho1
EP-9	34.68	34.83	34.81	34.82
OPY-9	22.63	22.63	22.45	22.32
HBPY-9	18.33	18.37	18.55	18.54
JTC-9	14.65	14.59	14.60	14.65
JCCU-9	10.11	10.00	10.01	9.96
CCU-9	9.34	9.25	9.30	9.23
JCSAPR-9	2.42	2.34	2.26	2.22
CSAPR-9	**1.67**	**1.62**	**1.57**	**1.52**
JTCTPR-9	3.76	3.68	3.59	3.51
TCTPR-9	2.09	2.05	1.99	1.91
JTDIC-9	10.70	10.83	10.91	10.90
HH-9	10.75	10.82	10.88	10.93
MFF-9	1.87	1.82	1.79	1.75

[a] Abbreviations: EP-9, enneagon; OPY-9, octagonal pyramid; HBPY-9, heptagonal bipyramid; JTC-9, Johnson triangular cupola J3; JCCU-9, capped cube J8; CCU-9, spherical-relaxed capped cube; JCSAPR-9, capped square antiprism J10; CSAPR-9, spherical capped square antiprism; JTCTPR-9, tricapped trigonal prism J51; TCTPR-9, spherical tricapped trigonal prism; JTDIC-9, tridiminished icosahedron J63; HH-9, hula-hoop; MFF-9, muffin. The values in boldface indicate the closest polyhedron according to the Continuous Shape Measures.

Physical Measurements/Characterization

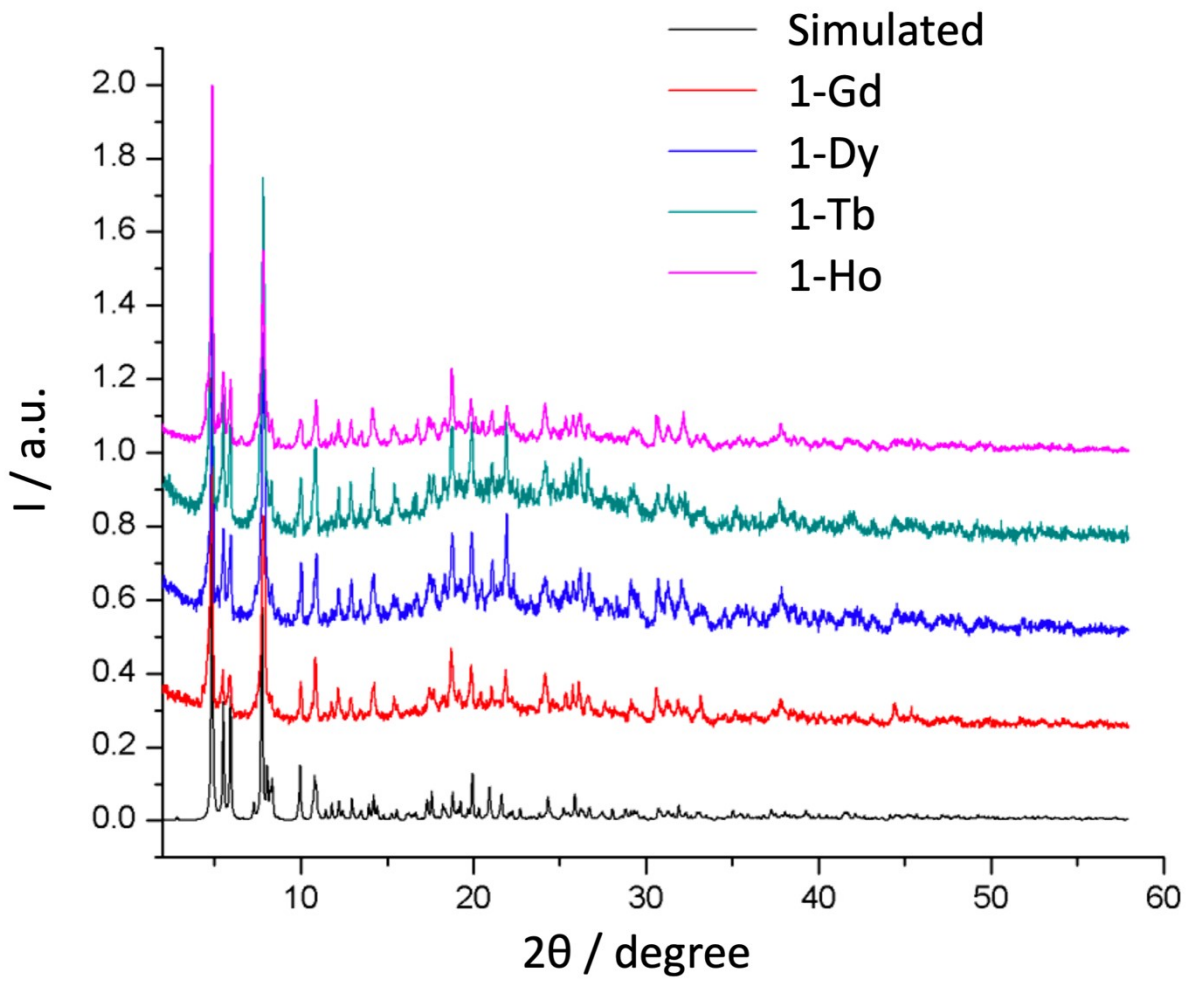

Fig. S1. Powder X-ray diffraction patterns of compounds **1**·MeCN/Gd, **1**·MeCN/Tb, **1**·MeCN/Dy and **1**·MeCN/Ho, along with the simulated pattern from the single crystal data.

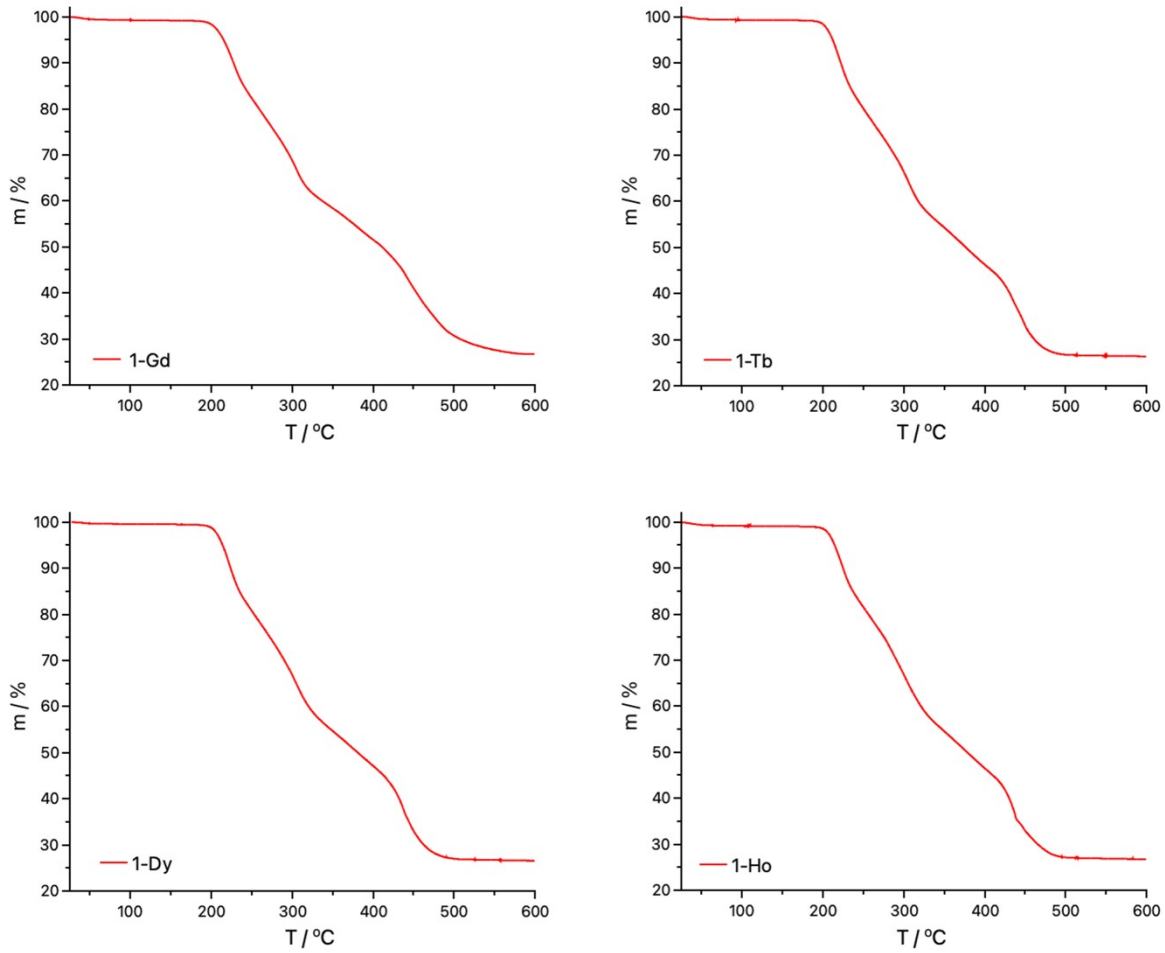

Fig. S2. TGA graphs of compounds **1**·MeCN/Gd, **1**·MeCN /Tb, **1**·MeCN/Dy and **1**·MeCN/Ho.

TGA analysis reveals that the thermal decomposition of the compounds proceeds through multistep processes which are completed at ~600 °C. The removal of the lattice solvent molecule is completed at ~210 °C and corresponds to ~2.7-2.9% of the materials' total mass. These values are in agreement with the corresponding calculated values for the removal of one MeCN solvent molecule from the four analogous compounds (2.9 %; see Table S3). The combustion of the coordinated molecules of the four analogues of **1**·MeCN/Ln (Ln = Gd, Tb, Dy, Ho) takes places through multistep processes which are completed at ~600 °C and accounts to ~71.9-72.1 % loss of their initial mass (calculated ~72.3-72.7%). The final residue is assigned to Fe_2O_3/0.5 Ln_2O_3 (Ln = Gd, Dy, Ho) or Fe_2O_3/0.25 Tb_4O_7 (calculated residue = 24.3-24.8%, found = ~25.2-25.3%).

Table S3. Calculated values for percentage mass loss of solvent removal and ligand combustion along with the experimental values obtained from TGA analysis of compounds **1**·MeCN/Gd, **1**· MeCN/Tb, **1**· MeCN /Dy and **1**· MeCN /Ho

Removal of Lattice Solvents				Ligand Combustion		Residual Oxide(s)		
Compound	Temperature (°C)	Experimental (Calculated) (%)	xMeCN	Temperature (°C)	Experimental (Calculated) (%)	Temperature (°C)	Experimental (Calculated) (%)	Formula
1·MeCN /Gd	r.t.-210	2.8 (2.9)	1	210-600	71.9 (72.7)	600	25.3 (24.3)	Fe_2O_3/0.5 Gd_2O_3
1·MeCN /Tb	r.t.-210	2.9 (2.9)	1	210-600	71.9 (72.4)	600	25.2 (24.7)	Fe_2O_3/0.25 Tb_4O_7
1·MeCN /Dy	r.t.-210	2.7 (2.9)	1	210-600	72.1 (72.5)	600	25.2 (24.6)	Fe_2O_3/0.5 Dy_2O_3
1·MeCN /Ho	r.t.-210	2.7 (2.9)	1	210-600	72 (72.3)	600	25.3 (24.8)	Fe_2O_3/0.5 Ho_2O_3

Magnetic measurements

Table S4. Chemical formulae and *J* coupling constants of Fe^{3+} - Gd^{3+} magnetic exchange interactions for selected heterometallic Fe^{3+}/Gd^{3+} complexes.

No	Complex[a]	J_{FeGd}	Refs.
1	$TBA_3[Fe_3Gd_2(N_3)_{15}(OH)_3(tipaH_3)_2]$	+0.267	1
2	$[\{Fe(3\text{-}MeOsalpn)Gd(NO_3)_3\}_2(\mu\text{-}O)]$	-3.25	2
3	$[Fe_3Ln(acac)_6(tea)_2]$	+0.73	3
4	$[Fe_2Gd_2(\mu_3\text{-}OH)_2(teaH)_2(O_2CPh)_6]$	+0.18	4
5	$[Fe_2Gd_2O(OH)(TBC[4])_2(DMF)_4(MeOH)_2(H_2O)_2]Cl$	-0.05	5
6	$Fe_2Gd[Fe_2Gd(L1)_2(O_2CC_3H_7)(H_2O)]$	+0.46	6
7	$[FeGd(bpca)_2(NO_3)_4]$	-0.199	7
8	$[Fe_4Gd_2(teaH)_4(N_3)_7\{O_2CC(CH_3)_3\}_3]$	+0.4	8
9	$[Fe_4Gd_2\{(py)_2CO_2\}_4(pdm)_2(NO_3)_2(H_2O)_2Cl_4]$	-6.0 / +2.8	9
10	$[Fe_2Gd_2(L2)_2(teaH)_2Cl_2](NO_3)_2$	+0.84	10
11	$[Fe_2GdO(O_2CPh)_4(dmem)_2(NO_3)]$	+0.85	11
12	$[Fe_2Gd_2(L5H_2)_4(NO_3)_2](ClO_4)_2$	+0.26	12
13	$Fe_4Gd_2(OH)_2(N_3)_2(bdea)_4\{O_2CC(CH_3)_3\}_4(NO_3)_2]$	-0.38 / +0.20	13
14	$[\{Fe_4(dea)_4Gd_4(deaH)_8(\mu_2\text{-}OMe)_4\}\cdot(NO_3)_4]$	+0.30 / +0.90	14
15	$[Fe_2Ln(O_2CPh)_3((py)_2CO_2)((py)_2C(OMe)O)_2(NO_3)Cl]$	+0.09	t. w.

[a]Lattice solvent molecules are omitted.

Abbreviations: t.w. = this work, TBA = tetrabutylammonium, $tipaH_3$ = triisopropanolamin, 3-$MeOsalpn^{2-}$ = N,N'-propylenebis(3-methoxysalicylideneiminate), acacH, acetylacetone, $teaH_3$ = triethanolamine, HO_2CPh = benzoic acid, TBC[4] = *p-tert*-Butylcalix[4]arene, $L1H_2$ = 2-hydroxy-3-methoxy-phenylsalicylaldimine, $HO_2CC_3H_7$ = butyric acid, bpcaH = bis(2-pyridilcarbonyl)amine, $HO_2CC(CH_3)_3$ = pivalic acid, $(py)_2C(OH)_2$ = gem-diol form of di-2-pyridyl ketone, $pdmH_2$ = pyridine-2,6-dimethanol, $L2H_2$ = N1,N3-bis(3-methoxysalicylidene)diethylenetriamine, $L3H_2$ = N,N'-bis(3-methoxysalicylidene)-1,3-diamino-2,2'-dimethyl-propane, $L4H_2$ = N,N'-bis(3-methoxysalicylidene)-1,2-diamino-2-methylpropane, dmemH = 2-{[2-(dimethylamino)ethyl]methylamino}ethanol, $L5H_4$ = (E)-2,2'-(2-hydroxy-3-((2-hydroxyphenylimino)methyl)-5-methylbenzylazanediyl)-diethanol, $bdeaH_2$ = N-butyldiethanolamine.

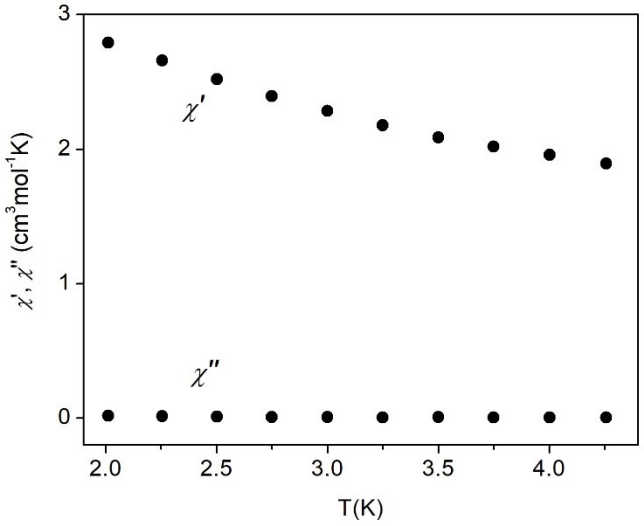

Fig. S3. Temperature dependence of χ' and χ'' from a powdered sample of **1**·MeCN/Ho under a zero external magnetic field and at 5111 Hz.

Mössbauer spectroscopy

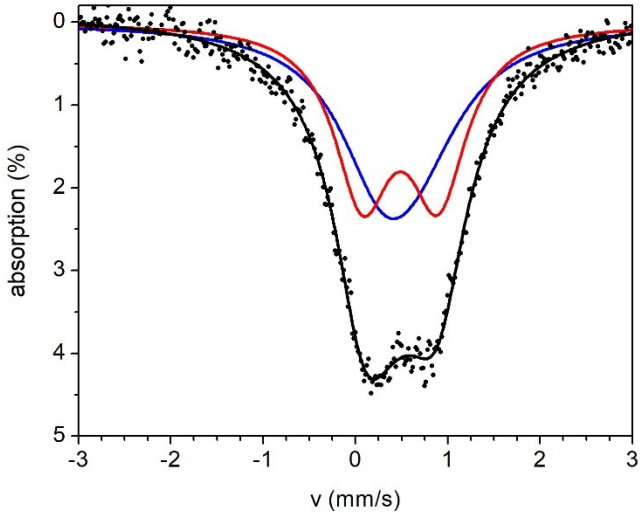

Fig. S4. Zero field Mössbauer spectra from a powder sample of **1**·MeCN/Gd at 80 K. Solid lines are theoretical spectra with the parameters listed in Table 2. Blue: doublet 1; red: doublet 2; black: sum.

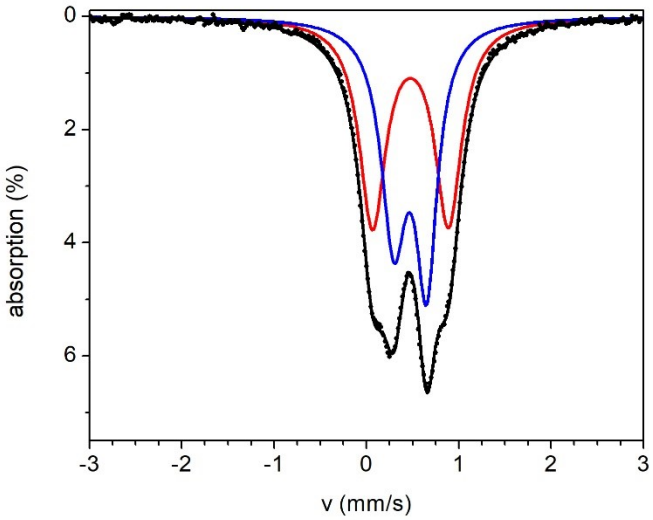

Fig. S5. Zero field Mössbauer spectra from a powder sample of **1**·MeCN/Tb at 80 K. Solid lines are theoretical spectra with the parameters listed in Table 2. Blue: doublet 1; red: doublet 2; black: sum.

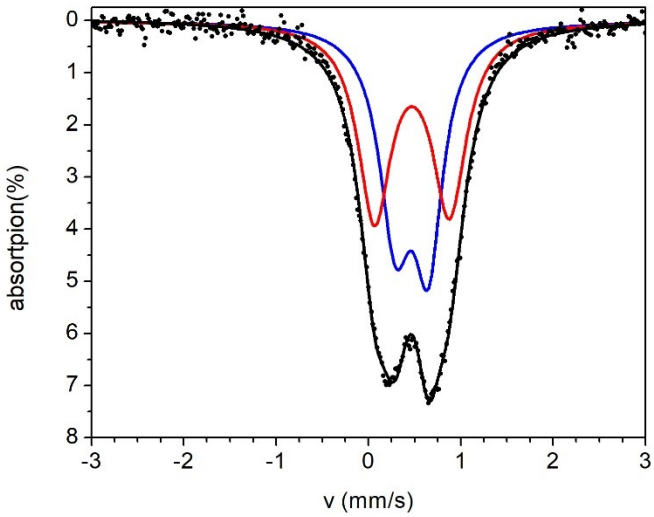

Fig. S6. Zero field Mössbauer spectra from a powder sample of **1**·MeCN/Ho at 80 K. Solid lines are theoretical spectra with the parameters listed in Table 2. Blue: doublet 1; red: doublet 2; black: sum.

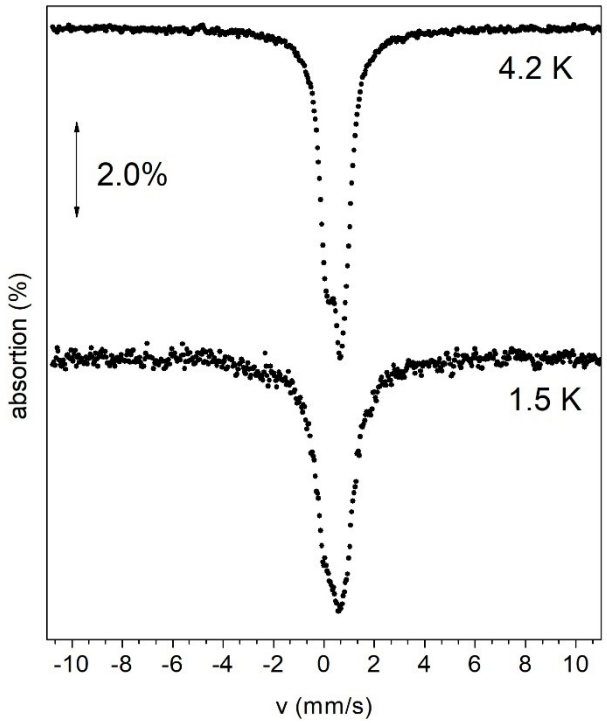

Fig. S7. Zero field Mossbauer spectra from powdered samples of **1**·MeCN/Tb at the indicated temperatures.

References:

1. S. F. M. Schmidt, M. P. Merkel, G. E. Kostakis, G. Buth, C. E. Anson and A. K. Powell, *Dalton Transactions*, 2017, **46**, 15661-15665.
2. M. Sarwar, A. M. Madalan, F. Lloret, M. Julve and M. Andruh, *Polyhedron*, 2011, **30**, 2414-2420.
3. N. F. Chilton, S. K. Langley, B. Moubaraki and K. S. Murray, *Chemical Communications*, 2010, **46**, 7787-7789.
4. A. Baniodeh, Y. Lan, G. Novitchi, V. Mereacre, A. Sukhanov, M. Ferbinteanu, V. Voronkova, C. E. Anson and A. K. Powell, *Dalton Transactions*, 2013, **42**, 8926-8938.
5. S. Sanz, K. Ferreira, R. D. McIntosh, S. J. Dalgarno and E. K. Brechin, *Chemical Communications*, 2011, **47**, 9042-9044.
6. W.-W. Kuang, C.-Y. Shao and P.-P. Yang, *Journal of Coordination Chemistry*, 2015, **68**, 1412-1422.
7. M. Ferbinteanu, F. Cimpoesu, M. A. Gîrţu, C. Enachescu and S. Tanase, *Inorganic Chemistry*, 2012, **51**, 40-50.
8. S. F. M. Schmidt, C. Koo, V. Mereacre, J. Park, D. W. Heermann, V. Kataev, C. E. Anson, D. Prodius, G. Novitchi, R. Klingeler and A. K. Powell, *Inorganic Chemistry*, 2017, **56**, 4796-4806.
9. H.-S. Wang, Q.-Q. Long, Z.-B. Hu, L. Yue, F.-J. Yang, C.-L. Yin, Z.-Q. Pan, Y.-Q. Zhang and Y. Song, *Dalton Transactions*, 2019, **48**, 13472-13482.
10. H.-S. Wang, C.-L. Yin, Z.-B. Hu, Y. Chen, Z.-Q. Pan, Y. Song, Y.-Q. Zhang and Z.-C. Zhang, *Dalton Transactions*, 2019, **48**, 10011-10022.
11. N. Singh, S. Das Gupta, R. J. Butcher and G. Christou, *Dalton Transactions*, 2017, **46**, 7897-7903.
12. P. Bag, J. Goura, V. Mereacre, G. Novitchi, A. K. Powell and V. Chandrasekhar, *Dalton Transactions*, 2014, **43**, 16366-16376.
13. S. G. Baca, J. van Leusen, M. Speldrich and P. Kögerler, *Inorganic Chemistry Frontiers*, 2016, **3**, 1071-1075.
14. A. Mondal, M. Raizada, P. K. Sahu and S. Konar, *Inorganic Chemistry Frontiers*, 2021, **8**, 4625-4633.